

Enhanced Chemoselective Hydrogenation through Tuning the Interaction between Pt Nanoparticles and Carbon Supports: Insights from Identical Location Transmission Electron Microscopy and X-ray Photoelectron Spectroscopy

Wen Shi,^{†,‡} Bingsen Zhang,^{*,†,‡} Yangming Lin,^{†,‡} Qi Wang,^{†,‡} Qiang Zhang,[§] and Dang Sheng Su^{*,†,‡}

[†]Shenyang National Laboratory for Materials Science, Institute of Metal Research, Chinese Academy of Sciences, Shenyang 110016, China

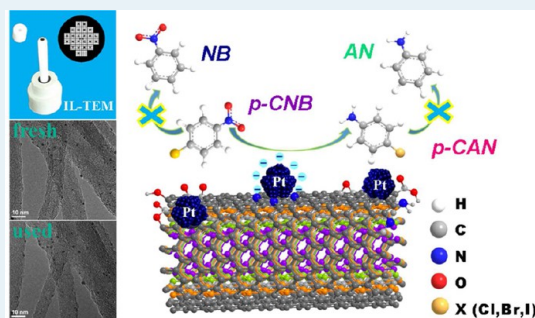
[‡]School of Materials Science and Engineering, University of Science and Technology of China, Hefei 230026, China

[§]Beijing Key Laboratory of Green Chemical Reaction Engineering and Technology, Department of Chemical Engineering, Tsinghua University, Beijing 100084, China

S Supporting Information

ABSTRACT: Ultrasmall-sized platinum nanoparticles (Pt NPs) (~1 nm) supported on carbon nanotubes (CNTs) with nitrogen doping and oxygen functional groups were synthesized and applied in the catalytic hydrogenation of nitroarenes. The advanced identical location transmission electron microscopy (IL-TEM) method was applied to probe the structure evolution of the Pt/CNT catalysts in the reaction. The results indicate that Pt NPs supported on CNTs with a high amount of nitrogen doping (Pt/H-NCNTs) afford 2-fold activity to that of Pt NPs supported on CNTs with oxygen functional groups (Pt/oCNTs) and 4-fold to that of the commercial Pt NPs supported on active carbon (Pt/C) catalyst toward nitrobenzene. The catalytic performance of Pt/H-NCNTs remained constant during four cycles, whereas the activity of the Pt/oCNTs was halved at the second cycle. Compared with Pt/oCNTs, Pt/H-NCNTs exhibited a higher selectivity (>99%) in chemoselective hydrogenation of halonitrobenzenes to haloanilines due to the electron-rich chemical state of Pt NPs. The strong metal–support interaction along with the electron-donor capacity of nitrogen sites on H-NCNTs are capable of stabilizing the Pt NPs and achieving related catalytic recyclability as well as approximately 100% selectivity. The catalyst also delivers exclusively selective hydrogenation toward nitro groups for a wide scope of substituent nitroarenes into their corresponding anilines.

KEYWORDS: nitrogen doping, IL-TEM, metal–support interaction, platinum nanoparticles, chemoselective hydrogenation



1. INTRODUCTION

Functionalized anilines are important industrial intermediates for a variety of pharmaceuticals, polymers, herbicides, and dyes. Nowadays, they are mainly obtained by using a vast of reducing agents, such as sodium hydrosulfite, hydrazine hydrate, or some unrecoverable non-noble metal ions (e.g., iron, tin or zinc), which always leads to serious environmental issues.¹ It is of great necessity to explore an environmentally friendly method to efficiently produce anilines. Catalytic hydrogenation of nitroarenes using molecular hydrogen (H₂) is the best choice for the production of functionalized anilines because of the clean and efficient production process. Nevertheless, the classical hydrogenation catalysts usually generate inevitable byproducts (Scheme S1), including hydroxylamines, nitroso, azo, and azoxy derivatives. This is due to the strong adsorption effect toward intermediate products.^{2–7} The chemoselective hydrogenation of nitroarenes with other reducible groups (e.g., –C=C, –OH, –Cl, –C=O, and –CN) on the benzene ring is also a great challenge.

In most cases, high selectivity is always achieved at the expense of activity by introducing either transition-metal salts

or additives that partly poison the active sites.^{8–10} Au and Ag-based catalysts with high selectivity require more harsh conditions due to its poor capacity of hydrogen dissociation.^{11–15} Pt-based catalysts appeared as a promising choice for chemoselective hydrogenation of nitroarenes because of their high dissociative capacity toward H₂.¹⁶ Furthermore, their versatile bimetallic structures,^{17,18} metal–support interaction,¹⁹ and well-controllable particle size^{20,21} also provide electronically modified Pt nanoparticles (Pt NPs), which is suitable for selective adsorption of the nitro group. Highly dispersed Pt NPs supported on various supports have been reported with high performance in the catalytic hydrogenation of nitroarenes (CHN) reactions.^{22–25} The role of the support is not only to well disperse the active sites but also to modulate the electronic structure for efficient reactant activation and product desorption.

Received: August 2, 2016

Revised: October 2, 2016

Carbon nanotubes (CNTs) are promising supports because they have high surface area, abundant π -electrons, and adjustable surface nucleation centers, which are in favor of providing the anchoring sites as well as regulating the chemical and electronic properties of noble metals.^{26–31} The hydrogenation activities of CNTs-supported noble metal NPs catalysts are highly dependent on the nature of functional species on the support surface, which can affect the particle size distribution (PSD), sintering resistance, and chemical state of metal NPs.^{32,33} Recently, most of the investigations focus on the interaction between small Pt NPs and heteroatom doping or functional species on CNT surface, especially in the electrocatalysis reactions.^{34,35} For instance, enhanced performance was assigned to the structural and electronic modification of Pt NPs induced by the nitrogen participation into the graphitic structure of CNT supports.^{36–38} However, the understanding on the critical role of modified CNTs on the supported Pt NPs in different catalytic reactions is still ambiguous, which strongly hinders the rational design of Pt/carbon catalyst for vast catalytic applications.

Herein, Pt NPs supported on pristine, oxygen functionalized, and nitrogen-doped CNTs were synthesized by ethylene glycol (EG) reduction^{39–41} method. The hydrogenation of nitroarenes is chosen as probe reaction to explore the interaction between Pt NPs and doping heteroatoms or functional groups on the support surface. The structural evaluation of the catalysts during the reaction was studied by the identical location transmission electron microscopy (IL-TEM) method. By comparing and quantifying a series of TEM images, the structural evolution of the catalysts was explored in detail, and the corresponding structure–function relationship was proposed.

2. EXPERIMENTAL SECTION

2.1. Support Synthesis. CNTs supplied by Tsinghua University were treated with water-diluted HCl (volume ratio is 1:1) before use. The average outer diameter range of most CNTs is between 15 and 20 nm. The oxygen-containing CNTs were obtained by treating the pristine CNTs with the mixture of concentrated HNO₃ and H₂SO₄ (with the volume ratio of 1:1) at 323 K for 2 h, labeled as oCNTs. Nitrogen-containing CNTs were obtained from the preoxidized CNTs by thermal treatment at 973 K for 4 h, with a heating rate of 10 K min⁻¹ in a furnace under NH₃ atmosphere, marked as L-NCNTs. CNTs with high N content were synthesized by a modified chemical vapor deposition (CVD) process over FeMo/Al₂O₃ catalyst and using imidazole as carbon/nitrogen feedstocks. In the catalytic CVD growth, catalysts (10 mg) uniformly distributed on quartz boats were heated to 973 K. Imidazole (5.0 g) were heated to 523 K in a separate tube furnace connected to that with the catalysts. Then, 10% NH₃ (diluted by Ar) was subsequently introduced to the linked furnace at a flow rate of 100 mL min⁻¹. After these two furnaces were cooled to room temperature, the as-obtained raw products were purified by concentrated HCl (100 mL HCl g product⁻¹) under vigorous stirring for 12 h. The products were collected by filtration, washed with H₂O until the pH of the filtrate reached 7, and dried at 393 K. The obtained N-doped CNTs were flagged as H-NCNTs.

2.2. Catalyst Preparation. The preparation of CNTs-supported Pt catalyst (Pt/CNTs) was carried out in EG solution containing H₂PtCl₆ as precursor salts. First, 100 mg of CNTs was dispersed in 50 mL of EG in a 100 mL round-bottom flask, and the mixture was ultrasonically treated to obtain a

homogeneous suspension. Then the suspension was allowed to cool to room temperature followed by the addition of 0.5 mL of EG solution of chloroplatinic acid (H₂PtCl₆·xH₂O) containing 2 mg mL⁻¹ of Pt, and the pH value was adjusted by dropping 1 mol L⁻¹ NaOH to pH = 9 with magnetic stirring to ensure good dispersion. Subsequently, the flask was placed in the center of an oil bath pot refluxing at 471 K for 5 h under the protection of N₂ atmosphere. After the suspension was cooled, the pH of the suspension was adjusted to pH = 2 by addition of 2 mol L⁻¹ HCl aqueous solution with vigorous stirring at room temperature. At the end, the product was collected by filter and washed several times with deionized water until it was free of Cl⁻. The final powders were washed with ethanol and subsequently dried at 353 K in a vacuum oven overnight. Pt supported on different supports were prepared by the same method, which were denoted as Pt/oCNTs, Pt/L-NCNTs, and Pt/H-NCNTs, respectively. The synthesis process of Pt/H-NCNTs with a different loading amount (0.5 to 3.0 wt %) was similar to the description above, in addition to the increasing precursor content.

2.3. Catalyst Characterization. Transmission electron microscopy (TEM) and high-angle annular dark field scanning TEM (HAADF-STEM) images were acquired by using an FEI Tecnai G2 F20 microscope equipped with HAADF-STEM detector. The TEM and STEM images obtained from IL-TEM method were operated at 120 kV. X-ray diffraction (XRD) patterns of CNTs and modified CNTs-supported Pt NPs catalysts were characterized by an X-ray diffractometer (D/MAX-2400) with Cu K α source at a scan rate of 2° min⁻¹. X-ray photoelectron spectroscopy (XPS) spectra were carried out by ESCALAB 250 instrument with Al K α X-rays (1489.6 eV, 150 W, 50.0 eV pass energy). N₂ physisorption was measured at 77 K using a Micrometrics ASAP 2020 instrument. UV-Raman spectroscopy was performed on powder samples by using a HORIBA LabRam HR Raman spectrometer. The excitation wavelength was 633 nm with a power of 0.2 mW. The loading amount of Pt was determined by a Leeman Laboratories Prodigy inductively coupled plasma mass spectrometry (ICP-MS). The real Pt contents for the different catalysts were measured by ICP through the method as the following description. Twenty milligrams of the catalysts was dispersed in 12 g of concentrated nitric acid in an autoclave, and the autoclave was kept in the oven at 453 K for 12 h. After the acid-treatment process, CNTs were completely decomposed. Lastly, the acid aqueous solution was diluted in a 50 mL volumetric flask.

2.4. Catalytic Reaction. The hydrogenation reaction was carried out in a 60 mL stainless autoclave with a Teflon inner layer. Before the activity test, 10 mg of catalysts were put into the autoclave, and 2 mmol nitrobenzene substrates dissolved in 4 mL of ethylbenzene were added into the autoclave; then the autoclave was heated to 313 K and kept for 30 min. Next, the autoclave was flushed with 5 atm hydrogen for three times. After being sealed, the autoclave was charged with H₂ until 5 atm, and then it was kept at 313 K for 20 min. Some of the reactions were also carried out at 313 or 333 K with a certain Pt/substrate ratio under 5 atm hydrogen pressure. The ambient nitrobenzene hydrogenation reaction was carried out in a 25 mL three-necked round-bottom flask by flowing H₂ in the bottom space of an ethylbenzene solution at 353 K. After the reaction, benzene methyl ether as external standard was added and the reactants were analyzed using gas chromatography (Agilent 7890A). The results are summarized in Tables 1–3, S3 and Figures 7, S6, S7.

2.5. Stability of Catalysts Investigated by the IL-TEM Method. Prior to the reaction, a very low amount of catalysts were deposited on the top side of a copper grid with alphabetical code. The grid was thereafter inserted in TEM to capture the initial state of the catalyst and track the accurate locations of the catalyst using the alphabetical code. The TEM grid acts as a shuttle, which allows the transfer of Pt/CNT catalysts between the electron microscope and the liquid reaction environment. Then the TEM grid was transferred to a specimen stage and participated the nitrobenzene hydrogenation reaction at 353 K under ambient pressure in a 25 mL three-necked round-bottom flask through the continuous bubble method (2 mmol nitrobenzene in 10 mL of ethylbenzene with 5 mg of catalysts and the activity data are presented in [Supporting Information](#); grid without catalyst tested as reference showed no activity toward nitrobenzene hydrogenation). After the reaction, the TEM grid was dried thoroughly and then transferred to the electron microscope again to acquire the TEM images at identical locations.

3. RESULTS AND DISCUSSION

3.1. Synthesis and Characterization of the Catalysts.

Pristine CNTs, oxygen-containing CNTs, and nitrogen-doped CNTs with low- and high-level nitrogen content were prepared as supports, designated as CNTs, oCNTs, L-NCNTs, and H-NCNTs, respectively. [Figure S1](#) exhibits the low-magnification TEM images of these four supports. H-NCNTs are typical bamboo-like structures due to the incorporation of a large amount of nitrogen in the bulk CNTs. The features of surface functional groups and doping species on these four kinds of CNTs are distinct, as revealed by XPS spectra ([Figures S2,S3 and Table S1](#)).

The treatment of concentrated HNO_3 and H_2SO_4 introduces some oxygen functional groups to the graphitic surface of CNTs, such as carbonyl (531.0 eV), carboxyl (532.1 eV), and hydroxyl (533.3 eV), as shown in [Figure S2a](#).⁴² Thermal treatment under NH_3 atmosphere at high temperature introduces a low amount of nitrogen species ([Figure S2b](#)). High-level nitrogen-doped CNTs can be achieved by using nitrogen-containing precursor during the CVD growth.⁴³ The nitrogen species on H-NCNTs are pyridinic (N_{Py} 398.1 eV), pyrrolic or amine (N_{Am} 399.8 eV), graphitic (N_{G} 400.6–400.8 eV), and oxidized (404.5) nitrogen, as revealed by XPS ([Figure S3](#)).⁴⁴ The supports were also characterized by Raman spectra and N_2 physisorption absorptions, as shown in [Figure S4 and Table S2](#).

A simple ethylene glycerol reduction method was chosen to homogeneously deposit tiny Pt NPs on the surface modified CNTs, marked as Pt/CNTs, Pt/oCNTs, Pt/L-NCNTs, and Pt/H-NCNTs. The Pt contents were examined as 0.8, 1.1, 1.0, and 1.1 wt %, respectively. It can be seen that Pt contents are slightly enhanced by introduction of oxygen groups or nitrogen heteroatoms on the surface of CNTs, which is ascribed to the more anchor sites for Pt NPs. [Figure 1](#) shows the representative low-magnification HAADF-STEM images of Pt-based catalysts. Highly dispersed and ultrasmall Pt NPs are observed. Statistical analysis of PSD was carried out by measuring ca. 350 Pt NPs (insets of [Figure 1](#)). The particle sizes are all in the range of 0.6–2.0 nm. The average sizes are 1.4, 1.4, 1.3, and 1.2 nm regarding Pt/CNTs, Pt/oCNT, Pt/L-NCNTs, and Pt/H-NCNTs, respectively. Pt/H-NCNTs catalyst displays an excellent dispersion of Pt NPs despite the smallest surface area. A more detailed analysis on PSD reveals that Pt NPs on H-NCNTs exhibited a little narrower PSD with 0.6–1.5 nm and a slightly

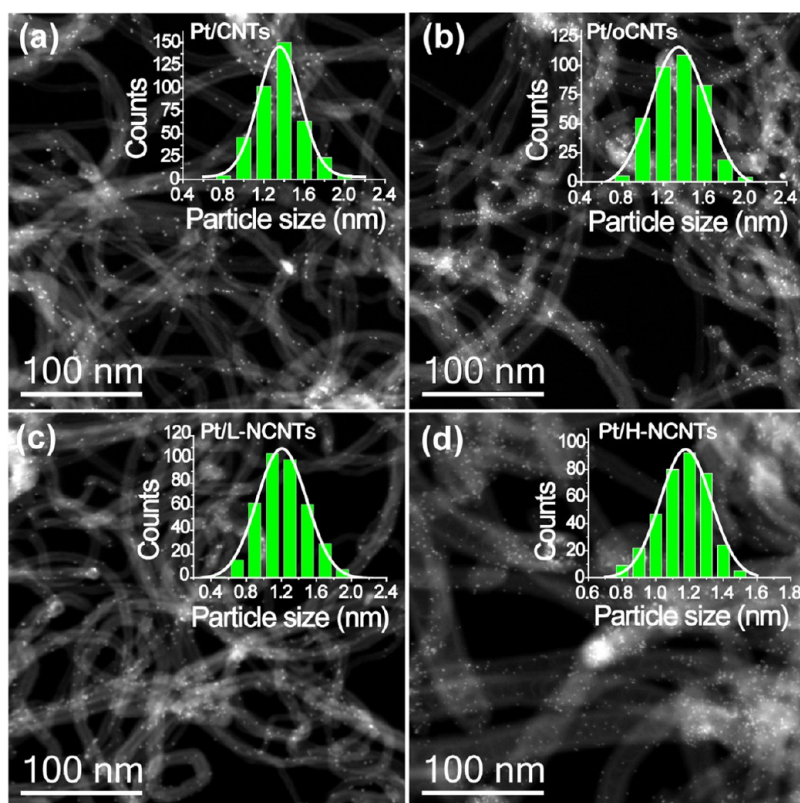


Figure 1. HAADF-STEM images of Pt/CNTs (a), Pt/oCNTs (b), Pt/L-NCNTs (c), and Pt/H-NCNTs (d). The insets are the corresponding PSD histograms.

smaller mean size of 1.2 nm. Usually, the particle size of Pt NPs supported on nanocarbons is related to the surface functional species amount and the interaction between the support and metal NPs.³¹ It indicates a strong metal–support interaction (SMSI) effect in Pt/H-NCNTs sample. Energy dispersive X-ray spectroscopy (EDX) elemental maps over different catalysts (Figure 2) illustrate the well-distributed O, N, and Pt in each sample.

X-ray diffraction (XRD) patterns of CNTs and Pt-based catalysts are shown in Figure 3. The main diffraction peaks at 26.3° and 42.2° are ascribed to (002) and (101) planes of the graphitic-type lattice, respectively. No obvious diffraction peak assigned to Pt NPs is found in XRD patterns, indicating that Pt NPs exist with very small size and good dispersion. In local regions, the selected area electron diffraction (SAED) patterns (Figure 4) show only the diffraction rings of CNTs. There are no diffraction spots regarding Pt NPs, illustrating ultrasmall size Pt NPs with low crystallinity stabilized on the CNT surface, which is in accordance with the XRD results. There are several weak peaks in the XRD pattern of H-NCNT besides the main CNT peaks (Figure 3b), which is attributed to the residual metal NPs capsulated into H-NCNTs. Based on aforementioned STEM, XRD, and SAED analyses, it indicates that Pt NPs existed as small particles with low crystallinity on the surface-modified CNTs.

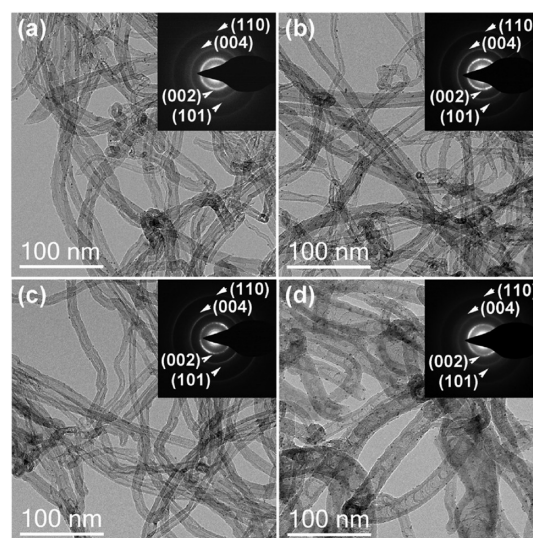


Figure 4. Low-magnification TEM images and corresponding SAED patterns of Pt/CNTs (a), Pt/oCNTs (b), Pt/L-NCNT (c), and Pt/H-NCNTs (d).

XPS is employed to investigate the dispersion of Pt NPs^{45,46} and the electronic interaction between supports and Pt NPs

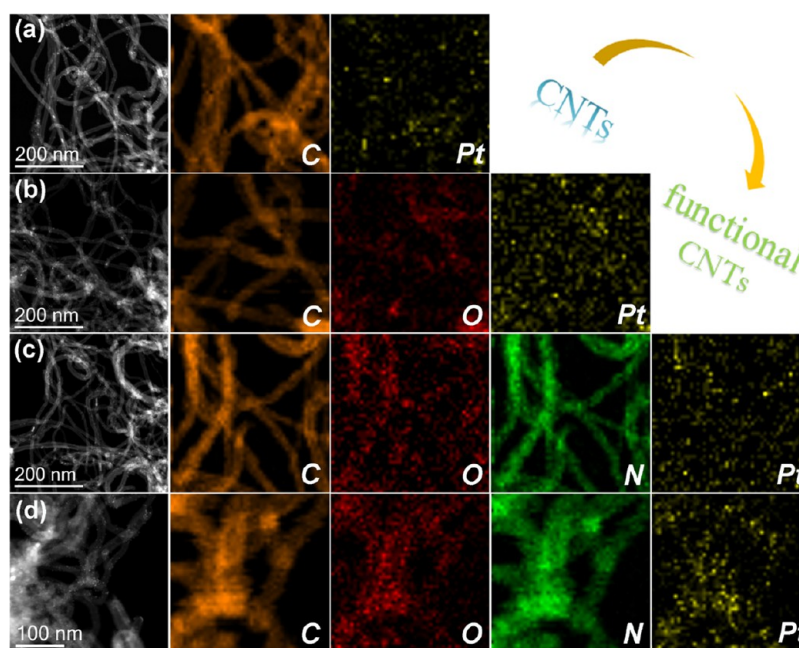


Figure 2. EDX elemental maps of Pt/CNTs (a), Pt/oCNTs (b), Pt/L-NCNTs (c), and Pt/H-NCNTs (d) samples.

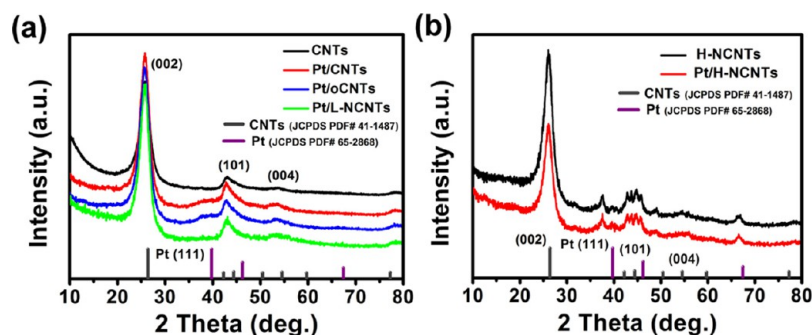


Figure 3. XRD patterns of the pristine CNTs, Pt/CNTs, Pt/oCNTs, and Pt/L-NCNTs (a), and H-NCNTs and Pt/H-NCNTs (b).

based on the intensity ratio and binding energy (BE) shift of Pt 4f.^{47,48} There is variation of surface Pt ratio on modified CNTs. Pt NPs supported on H-NCNTs exhibits the highest surface exposure of Pt content, which is mainly attributed to the lowest specific surface area among the samples (Table S1). The Pt 4f XPS spectra of the series catalysts (Figure 5) present

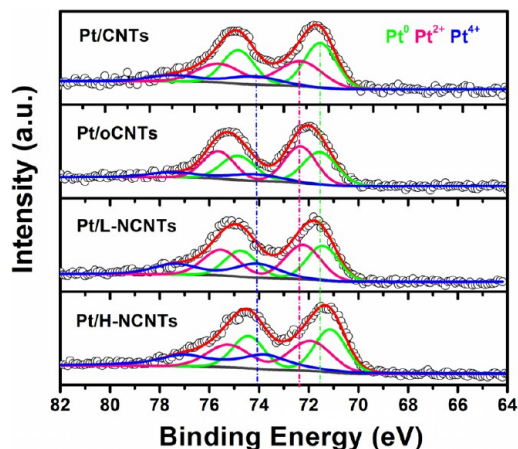


Figure 5. Pt 4f XPS spectra of Pt/CNTs, Pt/oCNTs, Pt/L-NCNTs, and Pt/H-NCNTs catalysts.

two main peaks at about 71.6 and 74.8 eV, corresponding to the spin-orbit split doublet of Pt 4f_{7/2} and 4f_{5/2}, respectively. Pt 4f spectra are deconvoluted into three components, including the predominant metallic Pt (Pt⁰), oxide states Pt (Pt²⁺), and Pt (Pt⁴⁺) in detail. The most intense doublet with BE of 71.5 eV (Pt 4f_{7/2}) and 74.8 eV (Pt 4f_{5/2}) is attributed to metallic Pt. Peaks at 72.3 eV (Pt 4f_{7/2}) and 75.6 eV (Pt 4f_{5/2}) are assigned to Pt²⁺, which anchored with the C–O groups on the surface of CNTs.^{49,50} The functional species on the CNT surface have great influence on the distribution of Pt species. Pt NPs supported on H-NCNTs tends to have more Pt⁰ than that of the other three catalysts, indicating that the introduction of nitrogen on CNTs is in favor of forming Pt⁰ species during the EG reduction process. The Pt²⁺ species on oCNTs and L-NCNTs can be ascribed to the surface-oxygen-containing groups, such as hydroxyl and carboxyl groups. Due to the weak reduction capability of EG, small amounts of Pt⁴⁺ still exist. The BE shift of Pt 4f is analyzed to unravel the electronic interaction between the distinct functional species and Pt NPs.

Accordingly, it is worthwhile to notice that Pt 4f BE toward the low-energy side can be observed obviously in Pt/H-NCNTs sample, but there is no obvious shift in Pt/L-NCNTs because of the low N content. In the case of Pt/H-NCNTs, the local electronic structure of Pt NPs can be significantly modified by the interaction with a large amount of N species. Compared with the N 1s XPS spectra of L-NCNTs and Pt/L-NCNTs (Figure S2b), a noticeable shift from the lower to the higher BE of the N 1s spectra was observed after Pt loading, which strongly implies the charge transfer from N species to Pt NPs. Thus, introduction of nitrogen species into the CNT structures generates an increased electron density of Pt, indicating a more electron richened chemical state of Pt NPs.

However, nitrogen-doped CNTs are always a complex system because of the coexistence of various N species, and it is still under debate as to which type of N functionality is responsible for the electronic interaction. Thus, a series of Pt/H-NCNTs with different Pt loading amount from 0.5 to 3.0 wt % were prepared to investigate the interaction between the distinct N species and Pt NPs. The Pt contents were determined as 0.2, 0.4, 0.9, 2.2 wt % by ICP. Figure S5 shows the STEM images of the series Pt/H-NCNTs catalysts, elucidating the homogeneously dispersed Pt NPs on the support. With the increasing of Pt loading amount, the sizes of Pt NPs show the tendency of growing up. XPS spectra (Figure 6 and Table S3) revealed that along with the gradually increasing Pt content, obvious shifting of Pt 4f BE toward the low-energy side can be observed, which is probably due to the size effect of Pt NPs.^{51,52} Accordingly graphitic N gradually shifts to the high-energy side while there is no change to the oxygen functional groups, strongly implying the electronic interaction is only occurred between N_G and Pt NPs. Such an electronic interaction is demonstrated to partially fill the valence band of Pt, resulting in the upshift of d-band center.⁵³

3.2. Catalytic Hydrogenation of Nitroarenes to the Corresponding Aniline. The hydrogenation of nitroarenes is used as a model reaction to probe the effects of the different surface-modified CNTs on the supported Pt NPs. The catalytic performance of nitrobenzene hydrogenation is summarized in Table 1 and Figure S6, with a blank experiment and the intrinsic activities of the supports (CNTs, oCNTs, L-NCNTs, and H-NCNTs). The conversion of nitrobenzene hydrogenation over distinct catalysts decreased in the following order: Pt/H-NCNTs > Pt/L-NCNTs > Pt/oCNTs > Pt/CNTs, and the activity of Pt/H-NCNTs, Pt/L-NCNTs, Pt/oCNTs, and

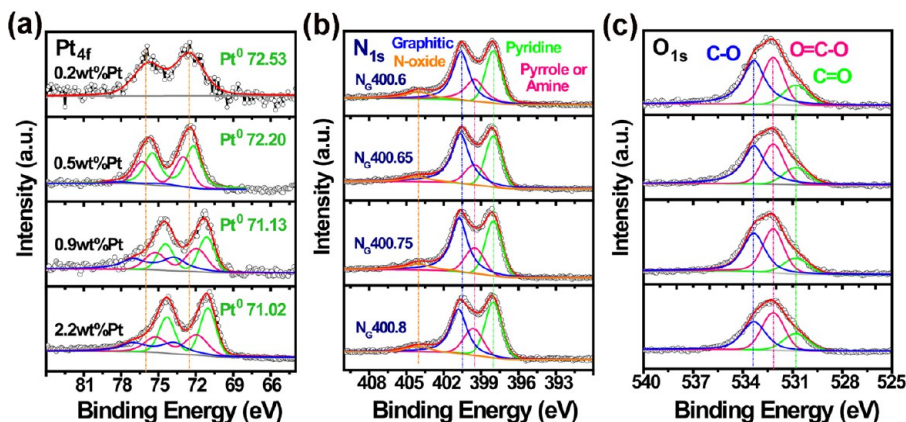


Figure 6. Pt 4f (a), N 1s (b), and O 1s (c) XPS spectra of Pt/H-NCNTs with varied Pt contents.

Table 1. Nitrobenzene Hydrogenation over Different Pt-Based Catalysts^a

entry	catalyst	conv. (%)	sel. (%)	activity data (mol _{AN} /(mol _{Pt} min))
1	blank	2.5		
2	CNTs	3.3		
3	oCNTs	3.1		
4	L-NCNTs	3.4		
5	H-NCNTs	3.3		
6	Pt/CNTs	37	93	67.1
7	Pt/oCNTs	63	93	114.3
8	Pt/L-NCNTs	76	96	142.3
9	Pt/H-NCNTs	98	99	189.3
10	5 wt % Pt/C	38	72	53.4

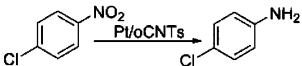
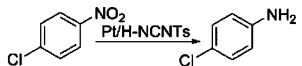
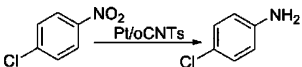
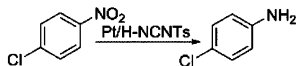
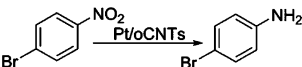
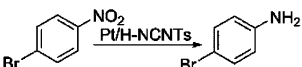
^aReaction conditions: $T = 40\text{ }^{\circ}\text{C}$, $P = 5\text{ atm}$, 10 mg of catalysts, 2 mmol nitrobenzene, 4 mL of ethylbenzene as solvent. Five wt % Pt/C commercial catalyst was purchased from Alfa Aesar.

Pt/CNTs catalysts normalized by Pt loading amount are 189.3, 142.3, 114.3, and 67.1 mol_{AN}/(mol_{Pt} min), respectively. Compared with the commercially available carbon-black-supported Pt catalyst (5 wt % Pt/C, purchased from Alfa Aesar), the used catalysts herein all performed much higher reactivity and more than 90% selectivity for aniline, which is attributed to the well-dispersed Pt NPs on the surface-modified CNTs synthesized by EG method. The reactions at 353 K under ambient condition (Figure S7) revealed that Pt/H-NCNTs displayed an enhanced activity. The activity (Table S3) of Pt/H-NCNTs catalysts with different loading amount are 215.8 (0.2 wt %), 209.1 (0.4 wt %), 188.8 (0.9 wt %), and 110.1 (2.2 wt %) mol_{AN}/(mol_{Pt} min),

respectively. The decreased activity with the increased Pt loading amount and the linear relationship between the activity of the surface-modified CNTs-supported Pt NPs catalysts and the amount of surface-exposed Pt (Figure S6b) indicate that the activity toward nitrobenzene hydrogenation mainly depends on the dispersion of the active metal, and a better dispersion of Pt can be achieved on H-NCNTs support, which is in accordance with the reported studies showing that the hydrogenation of nitrobenzene over Pt-supported catalysts appears to be size insensitive.^{54–56}

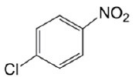
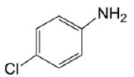
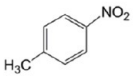
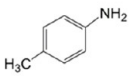
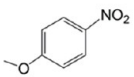
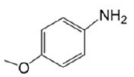
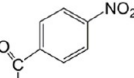
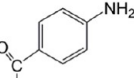
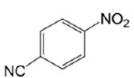
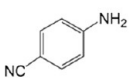
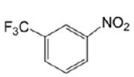
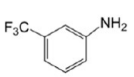
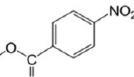
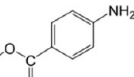
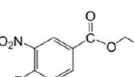
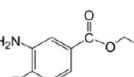
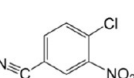
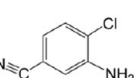
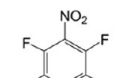
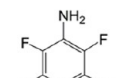
When the halonitrobenzene is used as a substrate, most Pt-based catalysts suffer from the hydrogenolysis of weak carbon–halogen (C–X) bond (dehalogenation in this work) reported previously,^{57,58} particularly at high conversions. Table 2 displayed the chemoselective hydrogenation of halonitrobenzene over Pt/oCNTs and Pt/H-NCNTs catalysts. Pt/H-NCNTs exhibits higher conversion as well as 100% selectivity toward chloronitrobenzene hydrogenation compared with Pt/oCNTs, avoiding C–Cl bond scissions even at a total conversion and no further decrease of chloroaniline products was observed over Pt/H-NCNTs even extending the reaction duration after complete conversion of chloronitrobenzene. In any case, the selectivity of Pt/H-NCNTs catalyst achieved 100% for the halonitroaromatic hydrogenation of nitro groups into the corresponding amino groups. However, Pt/oCNTs showed lower selectivity (95, 93, and 89% for chloro-, bromo-, and iodo- substrates, respectively) toward nitro group at the total conversion of substrates, and the selectivity decreased following the order of Cl^- , Br^- , I^- , which is in agreement with the susceptibility to hydrogenolysis induced by the increased atomic

Table 2. Chemoselective Hydrogenation of Halonitrobenzenes over Different Catalysts

Entry	Reaction	Conversion (%) [t(h)]	Selectivity (%)
1		65[0.5] ^[a]	95 ^[a]
2		95[0.5] ^[a]	100 ^[a]
3		98[1.5] ^[b]	95 ^[b]
4		98[1.5] ^[b]	100 ^[b]
5		99[2] ^[b]	93 ^[b]
6		99[2] ^[b]	100 ^[b]
7		100[2] ^[c]	89 ^[c]
8		100[2] ^[c]	100 ^[c]

^aReaction conditions: $T = 40\text{ }^{\circ}\text{C}$, $P = 5\text{ atm}$, Pt/substrate = 0.025%. ^bReaction conditions: $T = 40\text{ }^{\circ}\text{C}$, $P = 5\text{ atm}$, Pt/substrate = 0.05%. ^cReaction conditions: $T = 40\text{ }^{\circ}\text{C}$, $P = 5\text{ atm}$, Pt/substrate = 0.1%, ethylbenzene as solvent.

Table 3. Chemoselective Hydrogenation of Different Substituted Nitroarenes over Pt/H-NCNTs Catalysts

Entry	Substrate	Product	Conversion (%) [t(h)]	Selectivity (%)
1			>99[2] ^[a] >99[0.5] ^[b]	>99 ^[a] >99 ^[b]
2			86[2] ^[a] 97[1] ^[b]	83 ^[a] 97 ^[b]
3			75[1] ^[a] >99[1] ^[b]	>99 ^[a] >99 ^[b]
4			76[2] ^[a] 98[1] ^[b]	>99 ^[a] >99 ^[b]
5			95[1] ^[c]	>99 ^[c]
6			>99[1] ^[c]	>99 ^[c]
7			>99[1] ^[c]	>99 ^[c]
8			>99[1] ^[c]	>99 ^[c]
9			>99[1] ^[d]	>99 ^[d]
10			94[2] ^[d]	>99 ^[d]

^aReaction conditions: $T = 80\text{ }^{\circ}\text{C}$, ambient pressure, Pt/Substrate = 0.025%. ^bReaction conditions: $T = 60\text{ }^{\circ}\text{C}$, $P = 5\text{ atm}$, Pt/Substrate = 0.025%.

^cReaction conditions: $T = 60\text{ }^{\circ}\text{C}$, $P = 5\text{ atm}$, Pt/Substrate = 0.05%. ^dReaction conditions: $T = 60\text{ }^{\circ}\text{C}$, $P = 5\text{ atm}$, Pt/Substrate = 0.1%, ethylbenzene as solvent.

number as well as electronegativity of halogen groups. The electronic-enriched chemical state of Pt NPs on H-NCNTs inhibits dechlorination, whereas the higher binding energy of Pt on oCNTs impels more active hydrogen species to attack C–X bond or produces specific absorption toward C–X groups, which therefore facilitates the dehalogenation of halonitrobenzene. This hypothesis supported by XPS results is consistent with the recently publications reported by Iihama et al.^{59,60} Figure S8 demonstrates that all the catalysts have a similar distribution of Pt species and that the electronic interaction is also preserved after the reaction. Herein, through tuning the interaction between Pt NPs and the heteroatoms doping or functional groups on CNT surface, high hydrogenation capacity with superior selectivity catalyst for halonitrobenzene can be achieved.

Following the success of nitrobenzene and halonitrobenzene hydrogenation over Pt/H-NCNTs, it may display good performance when extended to other substituted nitroarenes. The results indicate that Pt/H-NCNTs catalyst illustrated excellent tolerance to a wide scope of substituted nitroarenes containing electron-donating or electron-withdrawing groups (Table 3). The catalyst showed high conversion as well as good selectivity to the corresponding anilines with the presence of $-\text{CH}_3$, $-\text{F}$, $-\text{CF}_3$, and $-\text{O}-\text{CH}_3$ groups (entries 2, 3, 6, and 10 in Table 3). Furthermore, Pt/H-NCNTs continued to preserve an excellent chemoselectivity toward the hydrogenation of nitroarene substituent with other reducible groups, such as $-\text{C}=\text{O}$, $\text{O}=\text{C}-\text{O}$, and $-\text{CN}$, which is the grand challenge for the application of selective hydrogenation of the substituted nitroarenes (entries 4, 5, 7, 8, and 9 in Table 3).

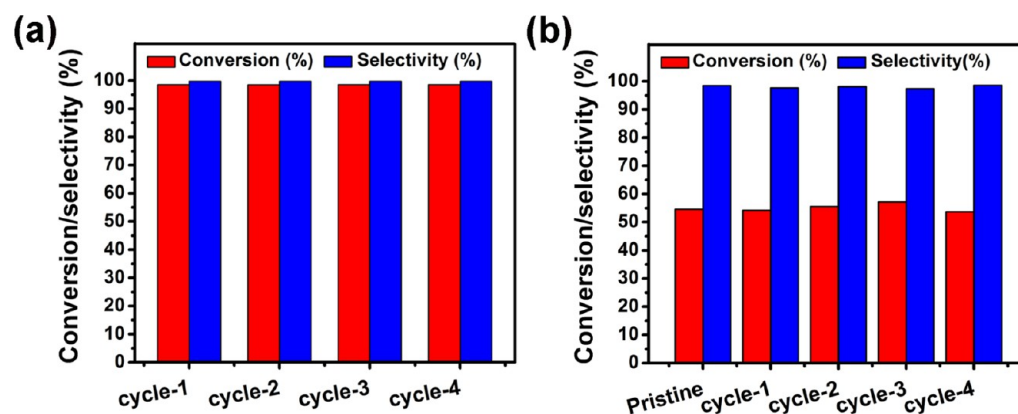


Figure 7. Recycling test of Pt/H-NCNTs for nitrobenzene hydrogenation to aniline at high conversion (a) and low conversion (b). (Reaction conditions: $T = 40\text{ }^{\circ}\text{C}$, $P = 5\text{ atm}$, Pt/substrate = 0.025%, 2 mmol nitrobenzene, 4 mL of ethylbenzene as solvent. Time = 20 min (a). Reaction conditions: $T = 40\text{ }^{\circ}\text{C}$, $P = 5\text{ atm}$, Pt/substrate = 0.01%, 4 mmol nitrobenzene, 4 mL of ethylbenzene as solvent. Time = 20 min (b)).

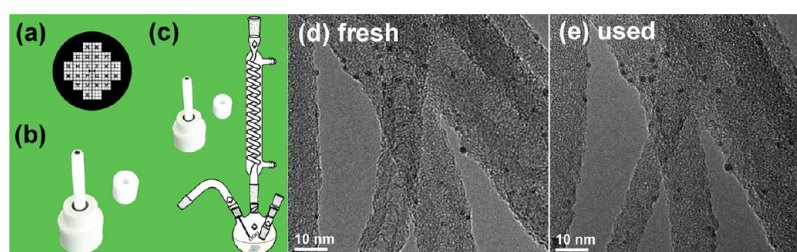


Figure 8. TEM grid with alphabetical code (a), specimen stage (b), and schematic diagram of the reactor (c). The TEM grid acts as a shuttle, which allows the transfer of the catalysts between the electron microscope and the liquid reaction environment. TEM images at identical location show the morphology of catalyst before (d) and after (e) reaction.

The major advantage of a heterogeneous catalyst is its stability under reaction conditions compared with a homogeneous catalyst. The conversion of nitrobenzene over Pt/H-NCNTs is 98.6% along with aniline selectivity of 99.8% after four successive runs, and it can be recovered from the reaction medium through simple filtration, as shown in Figure 7a. The catalyst stability was further demonstrated at a low conversion, as shown in Figure 7b. While Pt/oCNTs suffered from a decrease in activity for the second use (conv. 47% and sel. 96%), implying the stronger anchoring effect of H-NCNTs support than that of oCNTs for Pt NPs. The separated Pt/H-NCNTs catalyst after the fourth reaction run was examined by ICP, TEM, and HAADF-STEM in sequence. The Pt contents were determined as 1.0 wt % after four cycles, close to the initial Pt content 1.1 wt %. Compared with the TEM and HAADF-STEM images of fresh Pt/H-NCNTs catalyst, the recycled catalysts do not show any obvious changes (Figure S9). The small-sized Pt NPs are still homogeneously dispersed on the surface of H-NCNTs, and the main PSD is 0.9–1.8 nm, identical to that of the fresh catalyst (0.8–1.6 nm).

3.3. Stability of the Catalysts Studied by IL-TEM Method. We use IL-TEM^{61,62} to follow the structure evolution and the stability of the catalysts, where identical locations of a catalyst NP before and after the treatment in liquid reaction conditions can be investigated and compared. IL-TEM method in liquid reaction for accurate investigation of the structure evolution is shown in Figure 8. The acquired TEM images of Pt/oCNTs and Pt/H-NCNTs catalysts at identical location before and after the reaction for 30 min are shown in Figure 9. Pt NPs coalescence due to the particle migration on the support surface occurred in Pt/oCNTs catalyst under reaction conditions, and the same phenomena are not observed in

Pt/H-NCNTs sample at the selected areas. TEM images of several subregions for these two catalysts at increasing magnifications were tracked for a reliable understanding and distinguishing the structure evolution between them under reaction conditions (Figure S11 for Pt/oCNTs and Figure S12 for Pt/H-NCNTs). A quantitative evaluation of the catalysts regions visualized in the IL-TEM images is shown in Figure 9d,h, which compares the PSD of the catalysts before and after the participation of the liquid reaction. The average particle size increases from 1.3 to 1.8 nm in Pt/oCNTs, whereas a slight change in Pt/H-NCNTs sample and more obvious particle detachment on Pt/oCNTs than that on Pt/H-NCNTs is observed. Particle detachment and migration are a consequence of a weak interaction between Pt NPs and support, indicating a more strong anchoring effect in H-NCNTs than that in oCNTs for Pt NPs. Long-term stability on Pt/H-NCNTs catalyst was also evaluated by this strategy at several selected regions in Pt/H-NCNTs, suggesting that the particle size and dispersion are barely changed before and after nitrobenzene hydrogenation with different time at an elevated temperature (353 K) under ambient atmosphere, as shown in Figures 10, S13 and S14. Pt NPs are well anchored on the surface of H-NCNTs, exhibiting excellent stability under reaction conditions, which is in consistency with the good cycling performance.

Aiming to reveal the structure–function relationship, traditional approaches based on the comparison between fresh and used catalysts in liquid phase reactions always reach firm conclusions in conjunction with extensive statistical evaluations by observing different locations of the sample, which are useful but not always straightforward.⁶³ Some structure changes (e.g., particle detachment, dissolution, or agglomeration, particle reconstruction or encapsulation, and carbon support

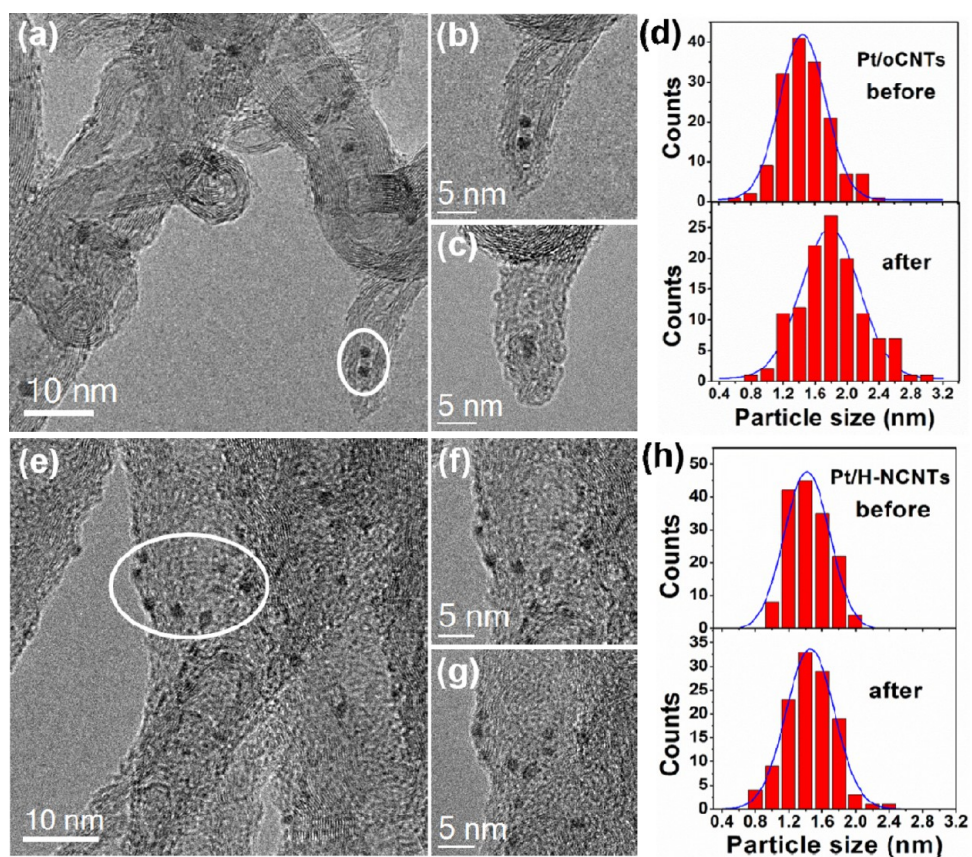


Figure 9. TEM images of Pt/oCNTs (a) and Pt/H-NCNTs (e) catalysts, the enlargement of selected area (outlined in white) before (b,f) and after the reaction for 30 min (c,g), and the corresponding PSD histograms (d,h) by quantifying a series of TEM images at identical locations.

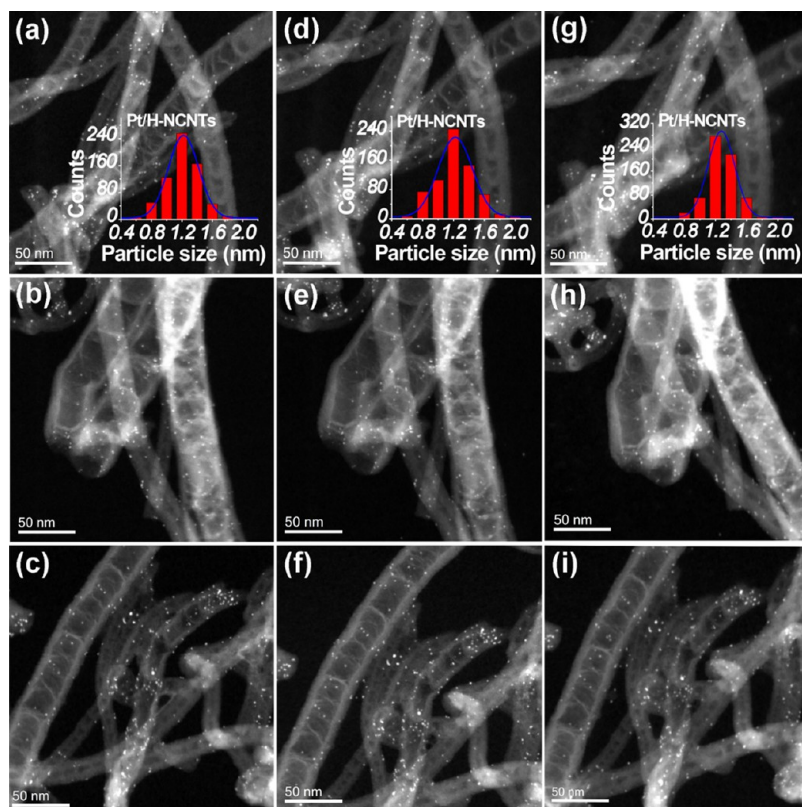


Figure 10. STEM images at identical location show the morphology of Pt/H-NCNTs catalyst before (a–c) and at the reaction time of 60 min (d–f) and 120 min (g–i). The insets are the corresponding PSD.

corrosion), however, are not directly traced and evidenced, originating from the reaction or the synthesis procedure. Herein, (i) IL-TEM is able to complement the routine microscopy investigations on the structure evolution and stability of catalysts, which provide detailed information on a catalyst at identical locations during liquid reactions; (ii) IL-TEM opens up new opportunities for the visualization of structural evolution on nanoscale and the establishment of the structure–function relationship; (iii) The simple and nondestructive IL-TEM can be extended to other reaction systems, where the conditions or chemical potential can never be mimicked in environmental TEM or using an environmental cell.⁶⁴

4. CONCLUSIONS

A series of Pt NPs supported on the surface-modified carbon nanotubes with uniform particle size distribution were synthesized by the ethylene glycol reduction method. The introduction of nitrogen substantially improved the catalytic performance toward nitrobenzene hydrogenation under mild conditions, which is ascribed to a better dispersion of Pt NPs. In addition, Pt/H-NCNTs catalyst exhibited superior stability under reaction conditions revealed by IL-TEM, which is consistent with the good recyclability, implying a strong anchoring effect of N species on CNT surface. Compared with Pt/oCNTs, Pt/H-NCNTs represented the exclusively selective hydrogenation toward nitro groups in halonitrobenzene hydrogenation, which is caused by the electronic interaction between Pt NPs and N_G species on CNT surface. The electron-donating effect of N_G species increases the electron density of the supported Pt NPs, such a binding energy shift resulting in a superior chemoselectivity hydrogenation capacity toward halonitroarenes. Furthermore, Pt/H-NCNTs catalyst also afforded high selectivity toward nitro group reduction to a wide scope of substituted nitroarenes (including –CH₃, –O–CH₃, –C=O, O=C–O and –CN groups). The current insight suggests a new route for rational designing high-performance catalysts through tuning the surface properties of the nanocarbon-based supports and thus enhancing the catalytic hydrogenation performance.

■ ASSOCIATED CONTENT

Supporting Information

The Supporting Information is available free of charge on the ACS Publications website at DOI: 10.1021/acscatal.6b02207.

Characterization of CNTs supports and the supported Pt catalysts, the catalytic performance of the modified CNTs-supported Pt NPs catalysts for nitrobenzene hydrogenation under ambient pressure, and the TEM results obtained from the IL-TEM method; characterizations include TEM images and corresponding SAED, N₂ adsorption–desorption isotherms and pore size distribution, Raman and XPS (PDF)

■ AUTHOR INFORMATION

Corresponding Authors

*E-mail: bszhang@imr.ac.cn. Tel: 86-24-83970027. Fax: 86-24-83970019.

*E-mail: dssu@imr.ac.cn. Tel: 86-24-23971577. Fax: 86-24-83970019.

Notes

The authors declare no competing financial interest.

■ ACKNOWLEDGMENTS

The authors gratefully acknowledge the financial support provided by the National Natural Science Foundation of China (Nos. 91545119, 21203215, 21133010, 51221264, and 21261160487), the Youth Innovation Promotion Association CAS (2015152), the Joint Foundation of Liaoning Province National Science Foundation and Shenyang National Laboratory for Materials Science (2015021011), and Strategic Priority Research Program of the Chinese Academy of Sciences (XDA09030103).

■ REFERENCES

- (1) Birkenstock, U.; Lachmann, B.; Metten, J.; Schmidt, H. United States Patent US4265834A, May 5, 1981.
- (2) Chary, K. V. R.; Srikanth, C. S. *Catal. Lett.* **2009**, *128*, 164–170.
- (3) Gao, Y.; Ma, D.; Wang, C.; Guan, J.; Bao, X. *Chem. Commun.* **2011**, *47*, 2432–2434.
- (4) He, D.; Jiao, X.; Jiang, P.; Wang, J.; Xu, B. Q. *Green Chem.* **2012**, *14*, 111–116.
- (5) Sun, Z.; Zhao, Y.; Xie, Y.; Tao, R.; Zhang, H.; Huang, C.; Liu, Z. *Green Chem.* **2010**, *12*, 1007–1011.
- (6) Liu, X.; Li, H. Q.; Ye, S.; Liu, Y. M.; He, H. Y.; Cao, Y. *Angew. Chem., Int. Ed.* **2014**, *53*, 7624–7628.
- (7) Boymans, E. H.; Witte, P. T.; Vogt, D. *Catal. Sci. Technol.* **2015**, *5*, 176–183.
- (8) Makosch, M.; Lin, W. I.; Bumbálek, V.; Sá, J.; Medlin, J. W.; Hungerbühler, K.; van Bokhoven, J. A. *ACS Catal.* **2012**, *2*, 2079–2081.
- (9) Furukawa, S.; Yoshida, Y.; Komatsu, T. *ACS Catal.* **2014**, *4*, 1441–1450.
- (10) Möbus, K.; Wolf, D.; Benischke, H.; Dittmeier, U.; Simon, K.; Packruhn, U.; Jantke, R.; Weidlich, S.; Weber, C.; Chen, B. *Top. Catal.* **2010**, *53*, 1126–1131.
- (11) Corma, A.; Serna, P. *Science* **2006**, *313*, 332–334.
- (12) Serna, P.; Corma, A. *ACS Catal.* **2015**, *5*, 7114–7121.
- (13) Shimizu, K. I.; Miyamoto, Y.; Kawasaki, T.; Tanji, T.; Tai, Y.; Satsuma, A. *J. Phys. Chem. C* **2009**, *113*, 17803–17810.
- (14) Sun, K. Q.; Hong, Y. C.; Zhang, G. R.; Xu, B. Q. *ACS Catal.* **2011**, *1*, 1336–1346.
- (15) Shimizu, K. I.; Miyamoto, Y.; Satsuma, A. *J. Catal.* **2010**, *270*, 86–94.
- (16) Rylander, P. *Catalytic Hydrogenation over Platinum Metals*; Elsevier: Amsterdam, 2012.
- (17) Ding, J.; Bu, L.; Zhang, N.; Yao, J.; Huang, Y.; Huang, X. *Chem. - Eur. J.* **2015**, *21*, 3901–3905.
- (18) Liu, J.; Zou, S.; Xiao, L.; Fan, J. *Catal. Sci. Technol.* **2014**, *4*, 441–446.
- (19) Chen, G.; Xu, C.; Huang, X.; Ye, J.; Gu, L.; Li, G.; Tang, Z.; Wu, B.; Yang, H.; Zhao, Z.; Zhou, Z.; Fu, G.; Zheng, N. *Nat. Mater.* **2016**, *15*, 564–569.
- (20) Lara, P.; Philippot, K. *Catal. Sci. Technol.* **2014**, *4*, 2445–2465.
- (21) Qiao, B.; Wang, A.; Yang, X.; Allard, L. F.; Jiang, Z.; Cui, Y.; Liu, J.; Li, J.; Zhang, T. *Nat. Chem.* **2011**, *3*, 634–641.
- (22) Wei, H.; Liu, X.; Wang, A.; Zhang, L.; Qiao, B.; Yang, X.; Huang, Y.; Miao, S.; Liu, J.; Zhang, T. *Nat. Commun.* **2014**, *5*, 5634–5641.
- (23) Tomkins, P.; Gebauer Henke, E.; Leitner, W.; Müller, T. E. *ACS Catal.* **2015**, *5*, 203–209.
- (24) Yoshida, H.; Igarashi, N.; Fujita, S. i.; Panpranot, J.; Arai, M. *Catal. Lett.* **2015**, *145*, 606–611.
- (25) Bergerand, C.; Yarulin, A.; Cárdenas Lizana, F.; Wärnå, J.; Sulman, E.; Murzin, D. Y.; Kiwi Minsker, L. *Ind. Eng. Chem. Res.* **2015**, *54*, 8659–8669.
- (26) Rodríguez Reinoso, F. *Carbon* **1998**, *36*, 159–175.
- (27) Planeix, J. M.; Coustel, N.; Coq, B.; Brotons, V.; Kumbhar, P. S.; Dutartre, R.; Geneste, P.; Bernier, P.; Ajayan, P. M. *J. Am. Chem. Soc.* **1994**, *116*, 7935–7936.

- (28) Wildgoose, G. G.; Banks, C. E.; Compton, R. G. *Small* **2006**, *2*, 182–193.
- (29) Li, Y. H.; Hung, T. H.; Chen, C. W. *Carbon* **2009**, *47*, 850–855.
- (30) Lv, R.; Cui, T.; Jun, M. S.; Zhang, Q.; Cao, A.; Su, D. S.; Zhang, Z.; Yoon, S. H.; Miyawaki, J.; Mochida, I.; Kang, F. *Adv. Funct. Mater.* **2011**, *21*, 999–1006.
- (31) Zhang, B.; Su, D. S. *ChemCatChem* **2015**, *7*, 3639–3645.
- (32) Motoyama, Y.; Lee, Y.; Tsuji, K.; Yoon, S. H.; Mochida, I.; Nagashima, H. *ChemCatChem* **2011**, *3*, 1578–1581.
- (33) Takasaki, M.; Motoyama, Y.; Higashi, K.; Yoon, S. H.; Mochida, I.; Nagashima, H. *Org. Lett.* **2008**, *10*, 1601–1604.
- (34) Bulushev, D. A.; Zacharska, M.; Lisitsyn, A. S.; Podyacheva, O. Y.; Hage, F. S.; Ramasse, Q. M.; Bangert, U.; Bulusheva, L. G. *ACS Catal.* **2016**, *6*, 3442–3451.
- (35) Li, L.; Hu, L.; Li, J.; Wei, Z. *Nano Res.* **2015**, *8*, 418–440.
- (36) Mabena, L. F.; Sinha Ray, S.; Mhlanga, S. D.; Coville, N. J. *Appl. Nanosci.* **2011**, *1*, 67–77.
- (37) Zhou, Y.; Neyerlin, K.; Olson, T. S.; Pylypenko, S.; Bult, J.; Dinh, H. N.; Gennett, T.; Shao, Z.; O'Hayre, R. *Energy Environ. Sci.* **2010**, *3*, 1437–1446.
- (38) Ning, X.; Yu, H.; Peng, F.; Wang, H. J. *Catal.* **2015**, *325*, 136–144.
- (39) Tao, A. R.; Habas, S.; Yang, P. *Small* **2008**, *4*, 310–325.
- (40) Fang, B.; Chaudhari, N. K.; Kim, M. S.; Kim, J. H.; Yu, J. S. *J. Am. Chem. Soc.* **2009**, *131*, 15330–15338.
- (41) Bonet, F.; Delmas, V.; Grugeon, S.; Urbina, R. H.; Silvert, P.; Tekcia-Elhissen, K. *Nanostruct. Mater.* **1999**, *11*, 1277–1284.
- (42) Qi, W.; Liu, W.; Zhang, B.; Gu, X.; Guo, X.; Su, D. *Angew. Chem., Int. Ed.* **2013**, *52*, 14224–14228.
- (43) Tian, G. L.; Zhao, M. Q.; Zhang, Q.; Huang, J. Q.; Wei, F. *Carbon* **2012**, *50*, 5323–5330.
- (44) Arrigo, R.; Hävecker, M.; Wrabetz, S.; Blume, R.; Lerch, M.; McGregor, J.; Parrott, E. P. J.; Zeitler, J. A.; Gladden, L. F.; Knop-Gericke, A.; Schlögl, R.; Su, D. S. *J. Am. Chem. Soc.* **2010**, *132*, 9616–9630.
- (45) Edmonds, T.; Mitchell, P. C. H. *J. Catal.* **1980**, *64*, 491–493.
- (46) Kerkhof, F.; Moulijn, J. J. *Phys. Chem.* **1979**, *83*, 1612–1619.
- (47) Wang, S.; Yang, F.; Jiang, S. P.; Chen, S.; Wang, X. *Electrochem. Commun.* **2010**, *12*, 1646–1649.
- (48) An, W.; Chuang, K. T.; Sanger, A. R. *J. Catal.* **2002**, *211*, 308–315.
- (49) Kundu, P.; Nethravathi, C.; Deshpande, P. A.; Rajamathi, M.; Madras, G.; Ravishankar, N. *Chem. Mater.* **2011**, *23*, 2772–2780.
- (50) Nie, R. F.; Wang, J. H.; Wang, L. N.; Qin, Y.; Chen, P.; Hou, Z. Y. *Carbon* **2012**, *50*, 586–596.
- (51) Mason, M. G.; Gerenser, L. J.; Lee, S. T. *Phys. Rev. Lett.* **1977**, *39*, 288–291.
- (52) Chen, W.; Ji, J.; Duan, X.; Qian, G.; Li, P.; Zhou, X.; Chen, D.; Yuan, W. *Chem. Commun.* **2014**, *50*, 2142–2144.
- (53) Liu, X.; Sui, Y.; Duan, T.; Meng, C.; Han, Y. *Catal. Sci. Technol.* **2015**, *5*, 1658–1667.
- (54) Sangeetha, P.; Shanthi, K.; Rao, K. S. R.; Viswanathan, B.; Selvam, P. *Appl. Catal., A* **2009**, *353*, 160–165.
- (55) Perez, M. M.; de Lecea, C. S. M.; Solano, A. L. *Appl. Catal., A* **1997**, *151*, 461–475.
- (56) Zhang, S.; Chang, C. R.; Huang, Z. Q.; Li, J.; Wu, Z.; Ma, Y.; Zhang, Z.; Wang, Y.; Qu, Y. *J. Am. Chem. Soc.* **2016**, *138*, 2629–2637.
- (57) Coq, B.; Tijani, A.; Figuéras, F. *J. Mol. Catal.* **1991**, *68*, 331–345.
- (58) Zhang, J.; Wang, Y.; Ji, H.; Wei, Y.; Wu, N.; Zuo, B.; Wang, Q. *J. Catal.* **2005**, *229*, 114–118.
- (59) Iihama, S.; Furukawa, S.; Komatsu, T. *ACS Catal.* **2016**, *6*, 742–746.
- (60) Motoyama, Y.; Lee, Y.; Tsuji, K.; Yoon, S. H.; Mochida, I.; Nagashima, H. *ChemCatChem* **2011**, *3*, 1578–1581.
- (61) Meier, J. C.; Katsounaros, I.; Galeano, C.; Bongard, H. J.; Topalov, A. A.; Kostka, A.; Karschin, A.; Schüth, F.; Mayrhofer, K. J. J. *Energy Environ. Sci.* **2012**, *5*, 9319–9330.
- (62) Schlögl, K.; Mayrhofer, K. J. J.; Hanzlik, M.; Arenz, M. J. *Electroanal. Chem.* **2011**, *662*, 355–360.
- (63) Shao, L.; Zhang, B.; Zhang, W.; Hong, S. Y.; Schlögl, R.; Su, D. S. *Angew. Chem., Int. Ed.* **2013**, *52*, 2114–2117.
- (64) Su, D. S.; Zhang, B. S.; Schlögl, R. *Chem. Rev.* **2015**, *115*, 2818–2882.